Available online at www.sciencedirect.com
ScienceDirect
Palaeogeography, Palaeoclimatology, Palaeoecology 249 (2007) 216–228
PALAEO
www.elsevier.com/locate/palaeo

Sea surface temperatures during the SW and NE monsoon seasons in the western Arabian Sea over the past 20,000 years

M.H. Saher *, F.J.C. Peeters, D. Kroon

Department of Paleoclimatology and Geomorphology, Institute of Earth Sciences, Vrije Universiteit Amsterdam, de Boelelaan 1085, 1081 HV Amsterdam, The Netherlands

Received 2 August 2006; received in revised form 23 January 2007; accepted 26 January 2007

Abstract

The western Arabian Sea is influenced by the seasonal southwest and northeast monsoon wind systems. In the modern day, SW monsoon induced upwelling of cold water leads to lowest SSTs in summer, while in glacial periods, weakened upwelling and increased cooling by NE monsoon winds may have resulted in lowest SST in winter. In order to reconstruct the western Arabian Sea seasonal sea surface temperature (SST) evolution during the monsoons over the past 20,000 years, a novel proxy is used that captures the contrast in seasonal SSTs. The presented proxy concerns the difference in δ^{18}O between two shallow dwelling species of planktonic foraminifera; *Globigerinoides ruber*, which calcifies throughout the year, and *Globigerina bulloides*, which mainly calcifies during SW monsoon driven upwelling. We convert this δ^{18}O difference to the difference in calcification temperature ($\Delta Tc_{rub-bul}$), and use it in combination with Mg/Ca-derived temperatures to reconstruct seasonal SSTs. We present the monsoon evolution record of Core NIOP929, located NW of the island of Socotra. Based on our results we distinguish three distinct modes. I) A glacial monsoon mode (20–13 ka BP) characterised by weakly negative $\Delta Tc_{rub-bul}$ values, and SW monsoon SSTs (T_{SW}) that are ~2 °C higher than NE monsoon SSTs (T_{NE}). This pattern is indicative for a weak SW monsoon and stronger cooling by glacial NE monsoon winds compared to the modern situation. II) A transitional mode (13–8 ka BP) characterised by $\Delta Tc_{rub-bul}$ values around 0, and thus a reduced difference between T_{SW} and T_{NE}. III) The modern monsoon mode, which started at 8 ka BP with the main shift toward low summer SSTs and high winter SSTs. The modern mode is characterised by $\Delta Tc_{rub-bul}$ values around +4 °C, indicative of a strong SW monsoon associated with strong upwelling, and weak influence of the NE monsoon on SST. We propose that measuring Mg/Ca on both species will improve the accuracy of the SST estimates.

Keywords: Seasonal SST; Arabian Sea; Monsoon; Planktonic foraminifera; Oxygen isotopes; Mg/Ca paleothermometry

1. Introduction

The Arabian Sea is under the influence of the Indian (also known as the west Asian) monsoon system (Brock et al., 1992; Fischer et al., 1996; Schott et al., 2001; Smith, 2001; Peeters et al., 2002). Differential heating of the ocean waters and continental land masses results in a seasonally reversing wind direction. In boreal summer, the low-pressure cell over Tibet causes the intertropical convergence zone (ITCZ) to shift northward, and induces a strong southwest monsoon. Ekman transport caused by

* Corresponding author. Fax: +31 20 5989941.
E-mail address: margot.saher@falw.vu.nl (M.H. Saher).

0031-0182/$ - see front matter © 2007 Elsevier B.V. All rights reserved.
doi:10.1016/j.palaeo.2007.01.014

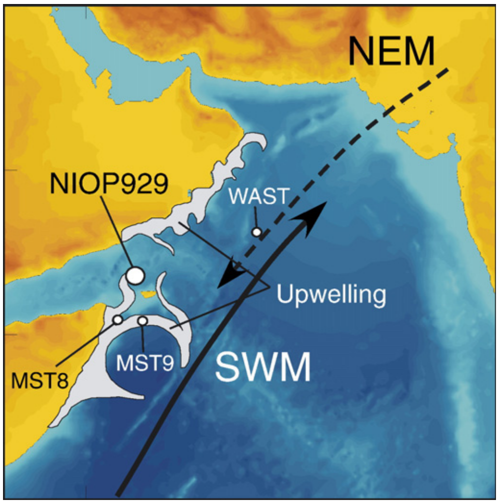

Fig. 1. Map of the Indian Ocean showing the location of Core NIOP929 and sediment traps MST8, MST9 (Conan and Brummer, 2000) and WAST (Nair et al., 1989; Curry et al., 1992). Arrows represent the approximate trajectories of the SW and NE monsoon (SWM and NEM, respectively). SW monsoon season upwelling areas (grey) off Somalia, Yemen and Oman are indicated in a sketchlike manner.

these southwestern winds induces upwelling of cold water, thereby lowering the summer sea surface temperature (SST). In winter, the ITCZ shifts southward, and the surface waters of the Arabian Sea are cooled by the winds of the northeast monsoon. Much previous work on the reconstruction of the western Asian monsoon system has focused on productivity proxies that are strongly related to upwelling intensity and hence mirror variability in mainly summer monsoon strength, such as the relative abundance of the upwelling planktonic foraminifer species *Globigerina bulloides* (Anderson and Prell, 1993; Gupta et al., 2003), total foraminiferal flux, δ^{18}O (Prell et al., 1992), δ^{15}N (Altabet et al., 1995; Ivanochko et al., 2005), or on changes in the coccolithophore assemblage (Beaufort et al., 1997). To capture the summer–winter contrast in SST, however, proxy information is required which provides information on the sea surface conditions of both monsoon seasons. Note that, for simplicity, we will use "summer" and "SW monsoon season" interchangeably in this text, and we do the same for the winter. There is evidence that such information is recorded in the fossil record of planktonic foraminifera: sediment trap and plankton tow studies (Curry et al., 1992; Conan and Brummer, 2000; Peeters and Brummer, 2002) reveal that the faunal composition changes seasonally. Most importantly, in summer the cold and nutrient-rich upwelled water promotes the cold water species *G. bulloides* to abound, while in winter, vertical mixing results in an increased abundance of *Globigerina falconensis*. The applicability of the relative abundance of *G. falonensis* as a measure for winter mixing is reflected in its sea floor distribution pattern in the Arabian Sea, which shows a maximum of more than 20% in the northeastern Arabian Sea, in the region of most intense winter mixing, and a decreasing percentage in a southwestward direction, to 2–5% near the upwelling area off Somalia (Schulz et al., 2002).

In this study we aim to address the western Arabian Sea seasonal sea surface temperature history over the last glacial–interglacial cycle. We propose a novel approach, using Mg/Ca-derived calcification temperatures in combination with the δ^{18}O composition of shells of different species of planktonic foraminifera. Ideally, the species *Globigerina bulloides* and *Globigerina falconensis* should be used to capture the respective monsoon signals. Unfortunately, as explained above, the relative abundance of *G. falconensis* is low in the western Arabian Sea. We thus have to rely on another species that is sufficiently abundant in western Arabian Sea sediments over the last 20,000 years to provide information on winter surface water conditions. The faunal record of the western Arabian Sea shows that *Globigerinoides ruber* can be used for this purpose. This species proliferates in both the summer and winter monsoon season and shows a relative

Table 1
^{14}C age calibration points

Depth (cm bsf)	No of lumped samples	^{14}C age	Error (1σ)	Species	Size fraction	Calibrated age (a BP)
21.0–22.5	3	1952	42	Mixed plankton [a]	250 μm+	1292
50.5–51.5	2	5550	46	*G. menardii*	250 μm+	5699
76.5–77.0	1	8560	50	*G. menardii*	355 μm+	8929
82.0–82.5	1	9249	51	*G. menardii*	355 μm+	9737
125.0–125.5	1	12,270	57	*G. menardii*	355 μm+	13,508
180.0–180.5	1	15,620	70	Mixed plankton [a]	250 μm+	18,313
210.5–211.0	1	17,380	85	*G. menardii*	355 μm+	19,920

[a] Mixed plankton: *G. menardii*, *G. bulloides*, *G. ruber*, *N. dutertrei*.

abundance between 9 and 17% (Conan and Brummer, 2000). This species, like *G. bulloides* but unlike *G. falconensis*, is a mixed layer dweller, which means we can deduce SSTs from the chemical properties of its shell.

In this study, we investigate how the isotopic composition of the species *Globigerina bulloides* and *Globigerinoides ruber* might be used as a proxy for the SST contrast between the summer and winter monsoon seasons. We first present and discuss our method, and then apply it to Core NIOP929 to reconstruct the western Arabian Sea seasonal SST history for the late glacial to Holocene time span, on millennial to centennial resolution. We combine this seasonal SST contrast proxy with the Mg/Ca-derived calcification temperature record of *G. ruber* to calculate the SW and NE monsoon season SSTs. A somewhat similar attempt was made by Van den Berg et al. (2002), who used the $\delta^{18}O$ of three species of planktonic foraminifera. In our approach presented here, we use only 2 planktonic species, in combination with the calcification temperature of one species. Measuring $\delta^{18}O$ and Mg/Ca of one species, combined with $\delta^{18}O$ of a species with a different seasonal preference, provides the minimal amount of proxy information to calculate seasonal SSTs. We propose that measuring Mg/Ca on both species will improve the accuracy of the SST estimates.

2. Material and methods

2.1. Core NIOP929

Core NIOP929 was recovered during the 1992–1993 Netherlands Indian Ocean Programme (NIOP) (van Hinte et al., 1995) in the western Arabian Sea (Fig. 1) (13°42, 21N; 53°14,76E) at a depth of 2490 m. The upper 210 cm of the 16.15 m long Core NIOP929 was cut into 0.5 cm slices. Sample availability prevented sampling the topmost 21 cm of this core. The age model of Core NIOP929 is based on nine AMS ^{14}C dates (Table 1). The age model is obtained by using linear interpolation between the ^{14}C age control points, and is described in

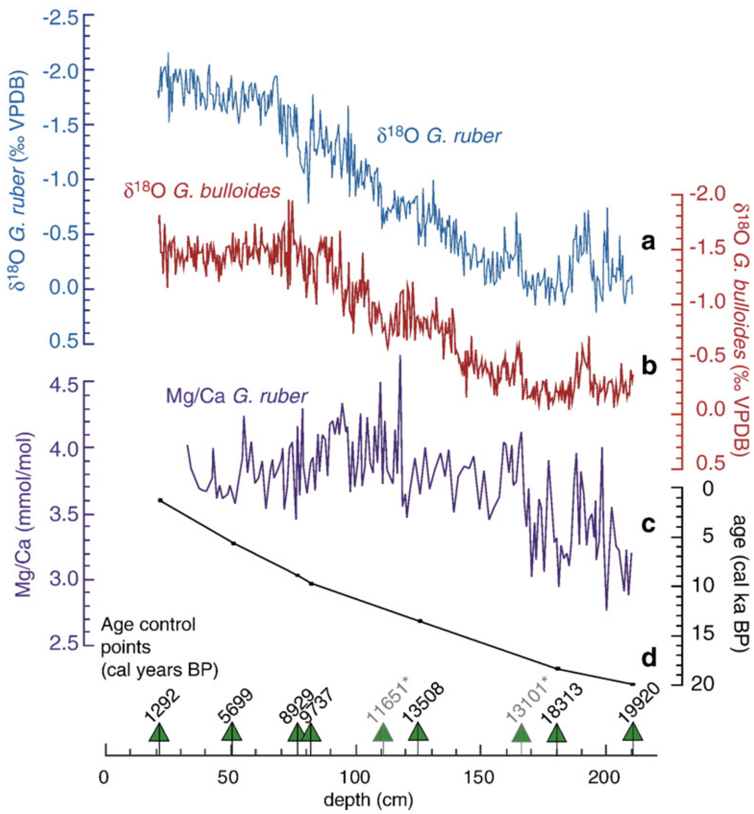

Fig. 2. The proxy data of Core NIOP929 plotted against depth. a: $\delta^{18}O$ of *Globigerinoides ruber*. b: $\delta^{18}O$ of *Globigerina bulloides*. c: The Mg/Ca ratio of *G. ruber*. d: The depth–age relationship of the given interval. At the base of the figure the ^{14}C age calibration points are depicted (calibrated to calendar age) on which the age model was based. Asterisks indicate age calibration points that were not considered. For a more detailed discussion see (Saher et al., in press).

more detail in Saher et al. (in press). The sampled interval has an average sedimentation rate of 10 cm/ka. Hence, the 0.5 cm sample spacing results in an average temporal resolution of 50 years (Fig. 2).

2.2. Stable isotopes

Thirty tests of *Globigerinoides ruber* and *Globigerina bulloides*, respectively, from the 250–355 µm fraction were used for stable isotope measurements. The tests were crushed, and 50 µg was used for a single measurement. The stable isotope measurements were performed on a Finnigan MAT252 equipped with a Kiel device. All isotope measurements were performed at the Institute of Earth Sciences at the Vrije Universiteit, Amsterdam. The external reproducibility of the δ^{18}O measurements is 0.07‰ (1σ). For a complete description of the methods used, see Saher et al. (in press).

2.3. Mg/Ca

The Mg/Ca record (Fig. 2) has a 1 cm sample spacing (every 2nd sample measured) over most of the record, with a total range between 0.5 and 3 cm, except in the late Holocene section where availability of foraminifera tests dictated sample spacing. For the Mg/Ca measurements twenty specimens of *Globigerinoides ruber* were used. The samples were prepared using the method described in Barker et al. (2003), with additional centrifuging for 5 min at 5000 rpm after dissolution in 350 µl 0.075M HNO_3. The measurements were performed at the Department of Earth Sciences of Cambridge University on a Varian Vista AX, as described in de Villiers et al. (2002). The Mg/Ca ratios were converted to calcification temperatures using the equation for *G. ruber* white 250–355 µm by Anand et al. (2003): Mg/Ca = 0.34 exp (0.102 * SST). The standard deviation of the residuals is 0.73 (1σ) using measurements from this size fraction (Anand, written comm., 2006). Possible effects of dissolution are discussed in Saher et al. (in press). In calculating modern annual average (flux weighted) calcification temperatures, we used the foraminifera flux data of Nair et al. (1989), Curry et al. (1992), and Conan and Brummer (2000).

2.4. Quantification of the seasonal temperature contrast

2.4.1. Calculation of $\delta^{18}O_w$, $\Delta Tc_{rub-bul}$ and Tc_{bul}

We are interested in obtaining seasonal SSTs, since this approach may provide a comprehensive view on monsoon evolution. The available data comprise the oxygen isotope composition of *Globigerinoides ruber* and *Globigerina bulloides*, and an independent Mg/Ca-derived SST estimate. The Mg/Ca-derived temperature of *G. ruber* reflects a flux weighted average calcification temperature of *G. ruber* (Tc_{rub}) over the time interval covered by each sample. From δ^{18}O and Mg/Ca data we calculate the average isotopic composition of the ambient sea water ($\delta^{18}O_w$), the difference in δ^{18}O of *G. ruber* and *G. bulloides* ($\Delta\delta^{18}O_{rub-bul}$), and use this to calculate $\Delta Tc_{rub-bul}$ and the calcification temperature of *G. bulloides* (Tc_{bul}). For calculating $\delta^{18}O_w$, we use the (adapted) formula of Kim and O'Neil (1997):

$$\delta^{18}O_w = (\delta^{18}O_{rub} + 0.5) - (25.778 - 3.333\sqrt{(43.704 + Tc_{rub})}) \tag{1}$$

Note that, in this equation, we corrected $\delta^{18}O_{rub}$ by 0.5‰ to account for the disequilibrium of δ^{18}O of *Globigerinoides ruber* with respect to the Kim and O'Neil (1997) temperature equation (Peeters et al., 2002).

$\Delta Tc_{rub-bul}$ is the difference between the recorded calcification temperatures of both species, which is proportional to the difference in $\delta^{18}O_{rub}$ and $\delta^{18}O_{bul}$. In general, temperature equations indicate that an increase of 1 °C results in a δ^{18}O decrease of 0.22‰. For an overview of this topic, we refer to Epstein et al. (1953), Erez and Luz (1983), and Bemis et al. (1998). We can therefore deduce:

$$\Delta Tc_{rub-bul} = \Delta Tc_{rub} - \Delta Tc_{bul} = \frac{\Delta\delta^{18}O_{rub-bul}}{-0.22}. \tag{2}$$

Tc_{bul} can be calculated from Tc_{rub} and $\Delta Tc_{rub-bul}$:

$$Tc_{bul} = Tc_{rub} - Tc_{rub-bul} \tag{3}$$

2.5. Calculation of T'_{SW} and T'_{NE}

We consider the temperature documented in the chemical composition of *Globigerinoides ruber* to be the result of the flux weighted average of the two seasonal temperatures, viz. the average ambient sea water temperatures during the SW monsoon season (T'_{SW}) and the NE monsoon season (T'_{NE}). We assume zero flux of *G. ruber* and *Globigerina bulloides* in the intermonsoon periods, based on sediment trap data (Curry et al., 1992; Conan and Brummer, 2000). Given r representing the fraction of the *G. ruber* population that calcified in summer, we can write:

$$\begin{aligned} Tc_{rub} &= rT'_{SW} + (1-r)T'_{NE} \quad [0<r<1], \text{ and} \\ Tc_{rub} &= \text{Mg/Ca-derived SST.} \end{aligned} \tag{4}$$

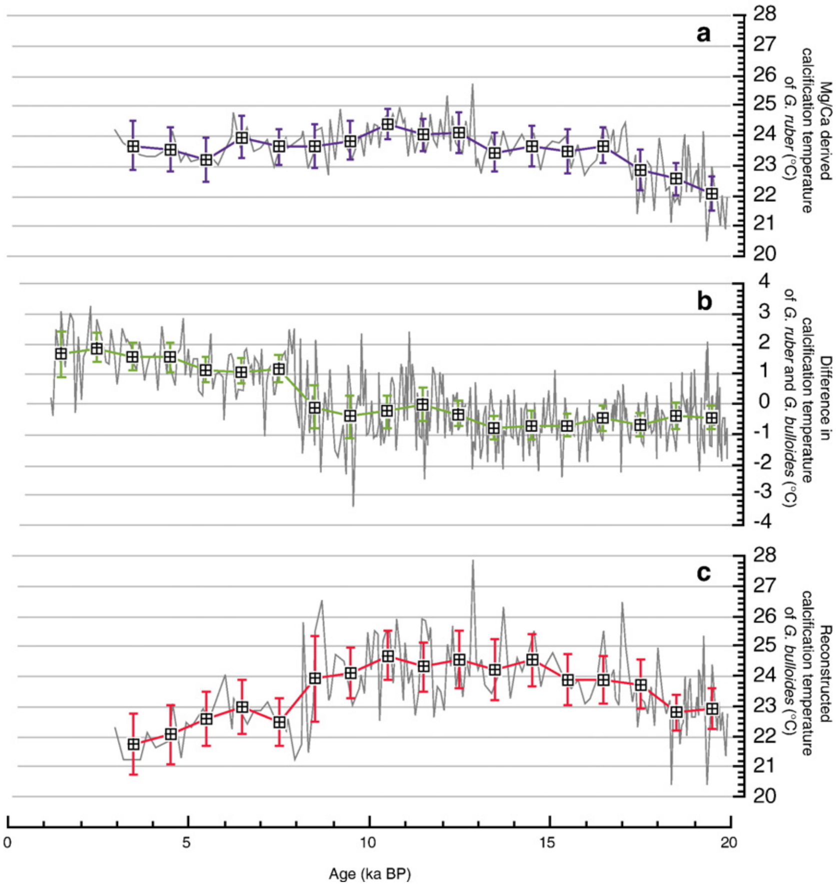

Fig. 3. The calcification temperatures of *Globigerinoides ruber* and *Globigerina bulloides* and their difference. Included is an overview of confidence interval analysis on calcification temperatures for 1000 year time slices. a: The Mg/Ca-derived calcification temperature estimates of *G. ruber*. b: The difference in calcification temperature of *G. ruber* and *G. bulloides* calculated from the difference in δ^{18}O. c: The calcification temperature of *G. bulloides*, calculated from the records shown in panels a and b. The grey line in all panels represents all data. In additions, in each panel 1000 year average estimates are given (boxes with crosses inside) that are plotted versus the midpoint of each 1000 year interval. The error bars represent the 95% confidence intervals on the mean temperature or, in panel b, the mean temperature difference for the 1000 year intervals. In our calculation of the 95% confidence intervals, we have included the error associated with the Mg/Ca temperature estimates of 0.73 °C (1σ), the long-term external reproducibility of oxygen isotope measurements of 0.07‰ (1σ), equivalent to 0.32 °C, and the error associated with the "within interval variability" of the measurements.

This can also be written as:

$$T'_{\mathrm{NE}} = \frac{\mathrm{Tc_{rub}} - rT'_{\mathrm{SW}}}{1-r} \tag{5}$$

For *Globigerina bulloides* we derive a similar type equation, in which b is the fraction of the population that calcified in the summer monsoon season, and $1-b$ is the fraction that calcified during the winter monsoon:

$$\mathrm{Tc_{bul}} = bT'_{\mathrm{SW}} + (1-b)T'_{\mathrm{NE}}. \tag{6}$$

Since sediment trap and plankton tow data indicate that *Globigerina bulloides* predominantly grows during the SW monsoon upwelling period, b is close to 1. With $b=1$, T'_{SW} becomes equal to $\mathrm{Tc_{bul}}$.

Subtracting Eqs. (4) and (6) results in:

$$\Delta\mathrm{Tc_{rub-bul}} = (r-b)T'_{\mathrm{SW}} + (b-r)T'_{\mathrm{NE}}. \tag{7}$$

Combining Eqs. (2) and (7), we get:

$$\frac{\Delta\delta^{18}\mathrm{O_{rub-bul}}}{-0.22} = (r-b)T'_{\mathrm{SW}} + (b-r)T'_{\mathrm{NE}}. \tag{8}$$

We then combine Eqs. (5) and (8):

$$\frac{\Delta\delta^{18}\mathrm{O_{rub-bul}}}{-0.22} = (r-b)T'_{\mathrm{SW}} + (b-r)\frac{\mathrm{Tc_{rub}} - rT'_{\mathrm{SW}}}{1-r}. \tag{9}$$

Table 2
Summary of the error analysis of the calcification temperatures

Interval	N Mg/Ca	Av. Tc_{rub} (°C)	1σ. Tc_{rub} (°C)	95% c.i. Tc_{rub} (°C)	Av. Tc_{bul} (°C)	1σ. Tc_{bul} (°C)	95% c.i. Tc_{bul} (°C)	N $\delta^{18}O$	Av. $\delta^{18}O_{rub}$ (‰)	1σ. $\delta^{18}O_{rub}$ (‰)	Av. $\delta^{18}O_{bul}$ (‰)	1σ. $\delta^{18}O_{bul}$ (‰)	$\Delta Tc_{rub-bul}$ (°C)	95% c.i. $Tc_{rub-bul}$ (°C)
0–1 ka	–	–	–	–	–	–	–	–	–	–	–	–	–	–
1–2 ka	–	–	–	–	–	–	–	11	−1.89	0.17	−1.52	0.20	1.67	0.76
2–3 ka	–	–	–	–	–	–	–	13	−1.86	0.14	−1.45	0.10	1.86	0.48
3–4 ka	4	23.7	0.41	0.8	21.6	0.61	1.0	13	−1.84	0.12	−1.49	0.10	1.58	0.46
4–5 ka	5	23.5	0.37	0.7	22.0	0.76	1.0	13	−1.78	0.12	−1.43	0.11	1.57	0.48
5–6 ka	4	23.2	0.16	0.7	22.5	0.37	0.9	14	−1.72	0.10	−1.47	0.10	1.16	0.41
6–7 ka	6	24.0	0.50	0.7	22.9	0.78	0.9	16	−1.74	0.12	−1.50	0.11	1.10	0.43
7–8 ka	7	23.6	0.33	0.6	22.4	0.68	0.8	16	−1.75	0.13	−1.49	0.11	1.18	0.45
8–9 ka	7	23.7	0.64	0.7	23.9	2.14	1.4	16	−1.53	0.17	−1.55	0.24	−0.09	0.70
9–10 ka	8	23.9	0.59	0.6	24.1	0.88	0.8	16	−1.26	0.23	−1.36	0.18	−0.41	0.68
10–11 ka	11	24.4	0.40	0.5	24.7	1.17	0.8	23	−1.30	0.15	−1.35	0.22	−0.24	0.53
11–12 ka	12	24.0	0.54	0.5	24.3	1.27	0.8	23	−1.08	0.20	−1.07	0.19	0.01	0.54
12–13 ka	11	24.1	0.86	0.7	24.6	1.40	0.9	23	−0.78	0.14	−0.85	0.15	−0.32	0.43
13–14 ka	7	23.4	0.48	0.6	24.3	1.09	1.0	23	−0.69	0.14	−0.86	0.15	−0.79	0.42
14–15 ka	6	23.7	0.45	0.7	24.6	0.67	0.9	23	−0.55	0.17	−0.70	0.17	−0.71	0.48
15–16 ka	6	23.5	0.53	0.7	23.9	0.60	0.8	22	−0.28	0.12	−0.44	0.12	−0.72	0.37
16–17 ka	8	23.7	0.50	0.6	23.9	0.81	0.8	23	−0.27	0.17	−0.37	0.12	−0.47	0.43
17–18 ka	12	22.9	0.96	0.7	23.8	1.25	0.8	23	−0.10	0.15	−0.24	0.13	−0.68	0.41
18–19 ka	17	22.6	0.86	0.5	22.8	0.95	0.6	33	−0.18	0.23	−0.26	0.16	−0.37	0.46
19–20 ka	17	22.1	0.89	0.5	23.0	1.18	0.7	36	−0.15	0.22	−0.25	0.12	−0.46	0.40

Key: *N*: number of data points in given interval, Av.: average, rub: *G. ruber*, c.i.: confidence interval on the mean, bul: *G. bulloides*.

Rewriting this produces the following equation for T'_{SW}:

$$T'_{SW} = Tc_{rub} + \frac{1-r}{r-b} \cdot \frac{\Delta\delta^{18}O_{rub-bul}}{-0.22}. \tag{10}$$

The value for T'_{SW} thus acquired is then introduced into Eq. (5), which results in a value for T'_{NE}.

It is noted that the calcification temperatures of *Globigerinoides ruber* and *Globigerina bulloides* (Tc_{rub} and Tc_{bul}), and therefore also T'_{SW} and T'_{NE}, are 1.3 °C to 1.7 °C lower than sea surface temperature (Peeters et al., 2002). The accuracy of these numbers is supernumerary in regard of the uncertainty in the method here presented, and therefore we correct with the average value of +1.5 °C.

$$T_{SW} = T'_{SW} + 1.5 \tag{11}$$

$$T_{NE} = T'_{NE} + 1.5. \tag{12}$$

2.6. Error analysis

In order to assess the validity of our results, we calculated the 95% confidence intervals for mean calcification temperatures over 1000 year intervals (Fig. 3). The error in Mg/Ca-derived mean Tc_{rub} depends only on the uncertainty of the regression (standard deviation of the residuals (1σ)=0.73 °C) and the observed variability within the 1000 year interval. The 95% confidence interval of the difference in calcification temperatures can be calculated by taking into account twice the external reproducibility of the mass spectrometer for $\delta^{18}O$ (1σ=0.07‰), and the variability within the intervals. As Tc_{bul} is calculated from Tc_{rub} and $\Delta\delta^{18}O_{rub-bul}$, both the errors in $\delta^{18}O$ and Mg/Ca as well as the variability within the interval have to be taken into account. The results are summarised in Table 2. The uncertainty of the calculated seasonal SSTs depends on the validity of the assumption that the past seasonal distribution of *Globigerinoides ruber* and *Globigerina bulloides* was similar to today. Unfortunately, no data on the past seasonal distribution of these species is available, and therefore we cannot provide an uncertainty estimate for the seasonal SST values. In the discussion we elaborate on the sensitivity of the equations to changes in seasonal distribution.

2.7. Estimates of r and b based on modern seasonal distributions of *Globigerinoides ruber* and *Globigerina bulloides*

Sediment trap data provide modern day seasonal distributions of *Globigerina bulloides* and *Globigerinoides ruber*. We based our values of *r* and *b* on nearby sediment traps MST8B, MST9E (Conan and Brummer, 2000) and WAST (Nair et al., 1989; Curry et al., 1992). To calculate the fractions of the population that calcify during the NE and SW monsoon seasons we need to first demarcate these seasons. As the used traps represent different monsoon years and localities, the monsoon seasons recorded in the three traps did not start and end on the same dates. It would therefore be preferable to define the monsoon seasons on the basis of foraminifera flux patterns. We then defined the monsoon seasons as periods in which per day $\geq 1\%$ of the total yearly flux are collected. For WAST, which covers a 1.5 year period, this exercise results in values for r of 0.5 to 0.6, and for b of 0.8 to 0.9. Traps MST8B and MST9E, however, did not cover an entire monsoon cycle. We therefore assumed that at the location of MST8B and MST9E, the NE monsoon season is restricted to the months January, February and March, and extrapolated the foraminiferal flux to the end of this period. Using the $\geq 1\%$ threshold for delimiting the SW and NE monsoon season, results in a value of 0.54 ± 0.08 for r, and 0.91 ± 0.06 for b. We get similar results, with a difference of 0.0 for b and 0.0 to 0.1 for r, if we use fixed (JAS and JFM) seasons for the extrapolated series of MST8B and MST9E. As we do not have constraints on the past seasonal distribution of the species we use the modern values for our reconstructions. As a check on the sensitivity of the method we evaluated the seasonal SST patterns calculated with different assumptions on seasonal distribution. As we realise the possibility that *G. bulloides* was less restricted to the SW monsoon season in the past than today, we calculated seasonal SST with a higher portion of the *G. bulloides* population calcifying in winter. We arbitrarily chose to additionally calculate the seasonal SSTs with a threefold increase of winter calcifying specimens of *G. bulloides*. Such a threefold increase of the modern value of 9% to 27% translates to a value for b of 0.73.

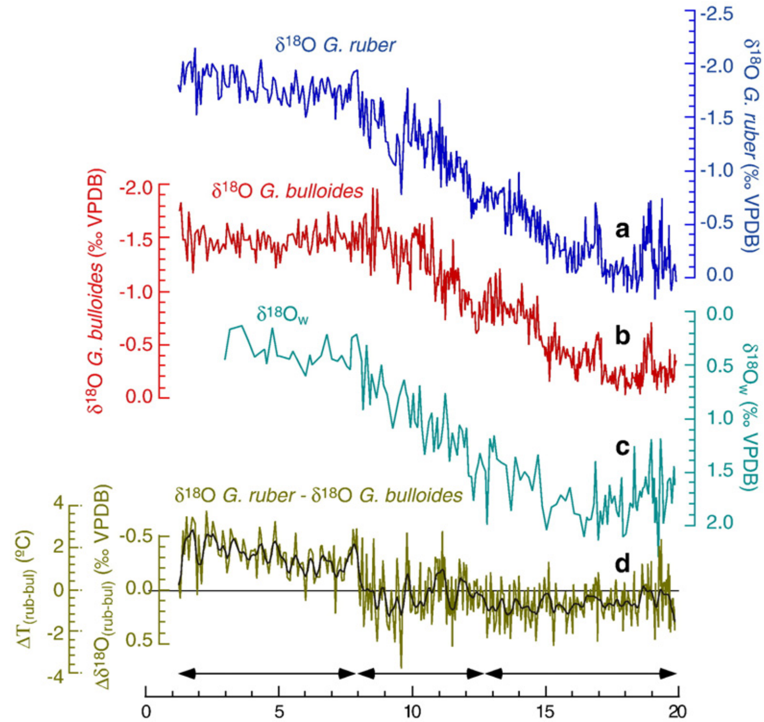

Fig. 4. The oxygen isotope records for *Globigerinoides ruber* and *Globigerina bulloides* of Core NIOP929, and the $\delta^{18}O_w$ and $\Delta\delta^{18}O_{rub-bul}$ or $\Delta Tc_{rub-bul}$ records that are derived from them. a: $\delta^{18}O_{rub}$. b: $\delta^{18}O_{bul}$. c: $\delta^{18}O_{w}$. d: The $\Delta\delta^{18}O_{rub-bul}$ or $\Delta TC_{rub-bul}$ record (both vertical axes given), as calculated from $\delta^{18}O_{rub}$ and $\delta^{18}O_{bul}$. For clarity, the records in panel d are plotted as raw data (green) and filtered data (black). Cutoff frequency of the filtered data is 1/500 years. In the $\Delta\delta^{18}O_{rub-bul}/\Delta Tc_{rub-bul}$ record three periods are distinguished; I: mainly negative $\Delta Tc_{rub-bul}$ values, II: large amplitude oscillations around 0, and III: mainly positive $\Delta Tc_{rub-bul}$ values. These periods are interpreted to reflect strong NE monsoon and weak SW monsoon (I), a transitional period (II) and the modern system characterised by weak NE monsoon and strong SW monsoon (III). (For interpretation of the references to colour in this figure legend, the reader is referred to the web version of this article.)

3. Results

3.1. $\delta^{18}O$ records

The oxygen isotope record of *Globigerinoides ruber* ($\delta^{18}O_{rub}$) ranges from +0.2‰ (LGM) to −2.2‰ (late Holocene), with average glacial and interglacial values of 0.0 and −1.8‰, respectively (Fig. 2). The glacial part of the Core NIOP929 record displays a distinct period of lower $\delta^{18}O_{rub}$ values at 19 ka BP. The deglaciation starts with a second period of low $\delta^{18}O_{rub}$, and is interrupted by two periods of increased values (14–13.5 ka BP and 13.5–12.2 ka BP). At 10 ka BP a pronounced increase in $\delta^{18}O_{rub}$ occurs, after which it decreases until 8 ka BP, from which $\delta^{18}O_{rub}$ values are relatively constant at ∼−1.8‰.

The oxygen isotope composition of *Globigerina bulloides*, $\delta^{18}O_{bul}$, ranges from +0.1‰ (LGM) to −2.0 (early Holocene), with glacial and Holocene averages of +0.2‰ and −1.5‰, respectively (Fig. 2). The glacial period displays a period of light $\delta^{18}O_{bul}$ at 19 ka BP, and a second period of light $\delta^{18}O_{bul}$ at the onset of the deglaciation, similar to those seen in the $\delta^{18}O_{rub}$ record. The gradual deglacial $\delta^{18}O_{bul}$ decrease is interrupted by two periods of subtly increasing values around 15 and 12 ka BP, and ends at 10 ka BP. Similar to $\delta^{18}O_{rub}$, the Holocene $\delta^{18}O_{bul}$ values are relatively stable, with an average value of −1.5‰. The calculated $\delta^{18}O_w$ record shows glacial values (Fig. 4) of on average +1.7‰ in the period 20 to 15 ka BP. At 15 ka BP the deglacial drop starts with a pronounced decrease, and it ends at 8 ka BP. Holocene values after 8 ka BP are on average +0.3‰.

3.2. Calcification temperatures

The Mg/Ca-derived Tc_{rub} record shows a stepwise warming with several relapses (Figs. 2, 3) from 20 ka BP to approximately 10 ka BP. Two centennial-scale warm periods, 19.3–18.7 ka BP and 17.1–16.4 ka BP, are apparent. These have been named Arabian Sea warm event 1 (ASW1) and 2 (ASW2), respectively, and discussed by Saher et al. (in press). After 10 ka BP the values drop faintly. Glacial values ranged between 22 °C and 23 °C (Fig. 3). During the deglaciation, temperature initially rose to 24 °C and subsequently decreased to 23.5 °C around 16 ka BP. At 13 ka BP the record shows an increase to 24 °C. The associated confidence

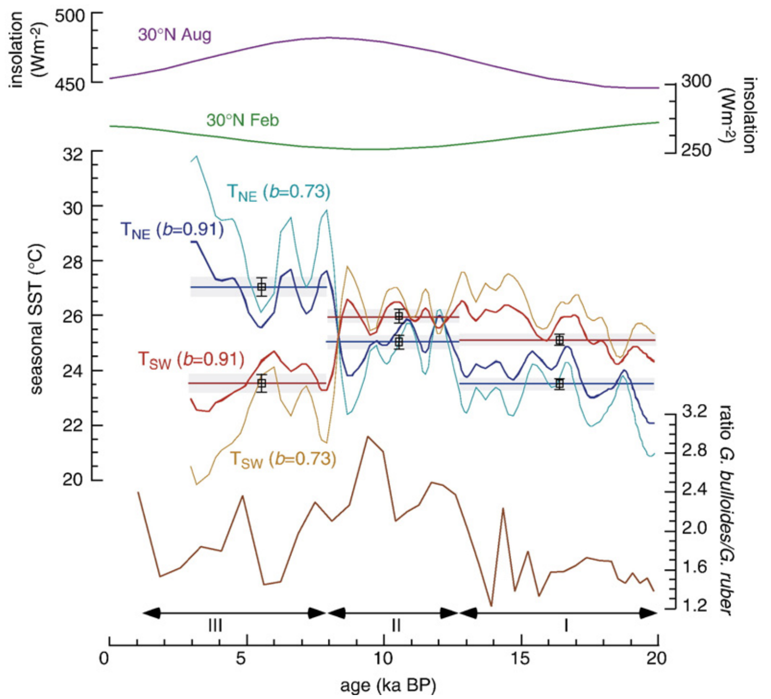

Fig. 5. Reconstructed seasonal SSTs of Core NIOP929, calculated using modern day values for r and b (b=0.91) and increased winter calcification of *Globigerina bulloides* (b=0.73). Results are smoothed for increased visibility. Horizontal lines are average seasonal SST over periods I, II and III calculated with modern day seasonal distribution (b=0.91). Grey blocks and error bars give the 95% confidence intervals on these average values. Seasonal SST calculated with b=0.73, for which no confidence interval is given, is provided as an indication for the sensitivity of the method to changes in seasonal distribution. Note that the pattern does not drastically change. Insolation curves for August and February are given as these months are at the centre of the summer and winter monsoon seasons.

intervals (Fig. 3) imply that most values are not statistically different from each other and are only valid at face value. The low glacial temperatures and the high temperatures during the YD, however, are robust. The warm YD seen in the records is discussed in detail in Saher et al. (in press).

$\Delta Tc_{rub-bul}$ (Fig. 4) mainly displays negative values (~−0.5 °C) in the glacial period and during the first part of the deglaciation, followed by a transitional period commencing at about 13 ka BP, in which $\Delta Tc_{rub-bul}$ is ~0 °C. At 8 ka BP the transitional period ends with a pronounced shift toward consistently positive values (~+1.5 °C). The Tc_{bul} record (Fig. 3) has higher variability than Tc_{bul} (total range: 20 °C–27.5 °C). Tc_{bul} rises from average values of 22 °C in the late glacial to 24 °C at 15 ka BP. At 8 ka BP, Tc_{bul} drops sharply to average values of 21.5 °C. The low glacial (20–18 ka BP) and interglacial (8–3 ka BP) temperatures significantly differ from the higher values in between.

3.3. Seasonal SSTs

The time series of T_{SW} and T_{NE}, which were smoothed (frequencies up to 1/500 years were filtered out) for better visibility, are shown in Fig. 5. The main drop in summer SST and the main rise in winter SST both take place around 8 ka BP. Before this shift, T_{NE} displays another warming from ~24 °C to ~25 °C at 12.5 ka BP. At 8 ka BP, T_{NE} rises from ~25 °C to ~28 °C.

T_{SW} also shows a warming trend from ~25 °C in the glacial part of the record (20–18 ka BP) to ~26 °C in the deglacial part (17–9 ka BP). At 8 ka BP, T_{SW} drops from ~26 °C to ~24 °C.

Fig. 5 shows that if the assumed fraction of *Globigerina bulloides* calcifying in winter is increased by threefold ($b=0.73$) compared to the modern day value, the total temperature range reconstructed increases by approximately a factor 2, but the overall shape of the curves as described above remains the same.

4. Discussion

4.1. Evaluation of the method

In this study we use the difference between $\delta^{18}O$ of upwelling species *Globigerina bulloides* ($\delta^{18}O_{bul}$) and *Globigerinoides ruber* ($\delta^{18}O_{rub}$), a species that nowadays calcifies throughout the year, as a proxy for seasonal temperature contrast ($\Delta\delta^{18}O_{rub-bul}$ or $\Delta Tc_{rub-bul}$), and hence for monsoon intensity.

A strong and/or cold NE monsoon would shift the $\Delta Tc_{rub-bul}$ values down, by cooling the winter sea surface, and thereby lowering the temperature recorded in the specimens of *Globigerinoides ruber* (Tc_{rub}) that calcify in winter. The strength and temperature of the NE monsoon winds would only minimally influence the calcification temperature of *Globigerina bulloides* (Tc_{bul}). A strong SW monsoon would lead to more vigorous upwelling, and thus lower Tc_{bul} of the entire *G. bulloides* population, and Tc_{rub} of the specimens that calcify in summer. As such, an increase in SW monsoon strength would shift the $\Delta Tc_{rub-bul}$ values up.

High $\Delta Tc_{rub-bul}$ values indicate a situation with strong (cold) summer upwelling and mild winters (strong SW monsoon, weak NE monsoon), while less negative values might either indicate weaker upwelling, or colder winters. Values around zero indicate a monsoonal mode with low seasonal contrast, and negative values are indicative for a situation where summer upwelling was weak, and winter SST was low (weak SW monsoon, strong NE monsoon).

4.2. Past seasonal distribution of *Globigerinoides ruber* and *Globigerina bulloides*

Based on the present day seasonal fluxes of *Globigerinoides ruber* and *Globigerina bulloides*, we assume in our approach a constant seasonal distribution of the species used. It is likely, however, that the seasonal fluxes have varied over time. The limiting factor for growth of *G. bulloides* is assumed to be food availability (Mortyn and Charles, 2003). As food is readily consumed in the surface waters, upwelled waters provide the highest food availability in the western Arabian Sea. The configuration of the Arabian Sea basin is such that Ekman transport due to SW monsoon winds, rather than NE monsoon winds, results in considerable coastal upwelling. Holocene NE monsoon winds are insufficiently strong to result in comparable eutrophia by means of deep winter mixing. Therefore, it seems reasonable to assume that in the Holocene period, *G. bulloides* calcified mainly during the SW monsoon season. The seasonal distribution of food in the Arabian Sea in (de)glacial times, however, is less well constrained. During the glacial period, low terrestrial temperatures and a larger Tibetan ice sheet (Kuhle, 1998) may have resulted in stronger and cooler NE monsoon winds. These could have resulted in stronger vertical mixing and concomitant erosion of the nutricline during winter (Reichart et al., 1998). As such, nutrient levels during the NE monsoon season may have been higher compared to the modern day, and possibly high enough for a thriving *G. bulloides* population. The glacial boundary conditions, however, would not only have amplified the NE monsoon, but also weakened the SW monsoon. This means upwelling in glacial periods could be suppressed to such a degree that T_{SW} is higher than T_{SW}. If in these periods *G. ruber* grew all year round, its annually averaged $\delta^{18}O$ values would still be lower than those of *G. bulloides*.

Low $\delta^{18}O$ values in the tests of *Globigerina bulloides* might point to higher temperatures of the upwelling water. This would not impede *G. bulloides*; a study by Kroon and Ganssen (1989) indicates that this species can grow in waters of up to 29.3 °C. Higher temperatures of the subsurface water may explain negative values of $\Delta Tc_{rub-bul}$.

4.3. Possible influence of factors other than temperature

Other factors beside SST changes could affect the $\delta^{18}O$ of foraminifera tests, and the $\Delta\delta^{18}O_{rub-bul}$ or $\Delta Tc_{rub-bul}$ values derived from them. These are variability in carbonate ion concentration ($[CO_3^{2-}]$); (Spero et al., 1997; Russell and Spero, 2000), and variability in $\delta^{18}O_w$, which is influenced by the evaporation/precipitation (E–P) balance. Subtracting the isotopic composition of the two species eliminates the inter-annual effect of $\delta^{18}O_w$. Intra-annual variations in $\delta^{18}O_w$, however, would affect our inferences. Nowadays, $\delta^{18}O_w$ in the western Arabian Sea is closely correlated with salinity ($r^2=0.96$; (Peeters, 2000)). In the western Arabian Sea, a typical intraseasonal difference in E–P driven salinity of the upper ~100 m water is 0.5 PSU (van Hinte et al., 1995; Peeters, 2000), with an average value of 35.7 PSU in summer and 36.2 PSU in winter. This would lead to a $\delta^{18}O$ difference of ~0.1‰ (and a $\Delta Tc_{rub-bul}$ change of ~0.5 °C) according to the relationships given by Delaygue et al. (2001): $\delta^{18}O=0.26*S-8.9$, and by (Jung et al., 2001): $\delta^{18}O=0.20*S-6.9$. The salinity dominated difference in $\delta^{18}O$ between the winter surface waters and the upwelling waters from a depth of ~200 m has a similar magnitude (Peeters, 2000). The influence on $\Delta\delta^{18}O_{rub-bul}$ or $\Delta Tc_{rub-bul}$ of $\delta^{18}O_w$ therefore is small compared to that of the temperature differences of several degrees °C that are routinely observed (e.g. Levitus et al., 1994) which result in $\delta^{18}O$ changes of over 1‰. However, we cannot constrain if these assumptions are valid over the time period covered by our records.

The intra-annual variability in surface water $[CO_3^{2-}]$ in the western Arabian Sea may be as high as 100 µmolkg^{-1} (Peeters et al., 2002). Assuming a modern seasonal distribution of the foraminifera, this fluctuation would result in a change in $\Delta Tc_{rub-bul}$ of ~0.5 °C, which is small compared to the effect of the seasonal temperature changes. Furthermore, Peeters et al. (2002) deduced very similar $[CO_3^{2-}]-\delta^{18}O$ relationships for *Globigerina bulloides* (−0.0025‰ µmol^{-1}kg^{-1}) and *Globigerinoides ruber* (−0.0022‰ µmol^{-1}kg^{-1}), indicating that differential response of the two different species to $[CO_3^{2-}]$ does not noticeably affect $\Delta\delta^{18}O_{rub-bul}$.

4.4. Monsoon evolution as derived from $\Delta Tc_{rub-bul}$

Based on the $\Delta Tc_{rub-bul}$ record over the past 20,000 years, three distinct periods are identified (Fig. 3): Period I, from the base of the record at 20 ka BP to 13 ka BP, in which $\Delta Tc_{rub-bul}$ was consistently negative, indicating summer SSTs were higher than winter SSTs. Period II, from 13 to 8 ka BP, which is a transitional period in which $\Delta Tc_{rub-bul}$ varied between −2 °C and +2 °C. Period III, lasting from 8 ka BP to the top of the record, which displays consistently positive values for $\Delta Tc_{rub-bul}$. This indicates a modern monsoon system that is characterised by strong SW monsoon winds and thus strong upwelling, and has lowest SSTs in summer.

4.5. Period I (20–13 ka BP)

In glacial period I, low (summer) solar insolation (Berger, 1978; Fig. 5) and extensive ice cover of the Tibetan Plateau (Kuhle, 1998) likely caused a weaker SW monsoon and stronger NE monsoon than in the Holocene. This monsoonal mode that is supported by previous studies, e.g. Fontugne and Duplessy (1986), Prell and Campo (1986), and Anderson and Prell (1993), would result in the described summer–winter SST contrast.

4.6. Period II (13–8 ka BP)

The increase of the SW monsoon signal in period II (Fig. 3) is also seen in ODP723 (Naidu and Malmgren, 1996), which show a sharp increase in upwelling indicators at 12 ka BP. The change from periods I to II is synchronous with a rise in Mg/Ca temperature (Fig. 3), which suggests the deglaciation had progressed to such a degree that the winter monsoon was faltering, yet the summer monsoon had not yet gained its full strength as observed in the late Holocene part of the record. These findings are in line with studies by Overpeck et al. (1996) and Naidu and Malmgren (2005). The transitional monsoonal mode characterizing period II (13 to 8 ka BP) is also seen in various terrestrial records from China (Zhou et al., 1996).

4.7. Period III (8–2 ka BP)

The pronounced shift at the boundary between period II and III (8 ka BP; Fig 4) marks the onset of the modern monsoon system in Core NIOP929. The shift occurred within a few centuries, suggesting that a (climatic) threshold level may have been reached that allowed the monsoon system to enter a different mode. The $\delta^{18}O$ data of the individual species reveal that the increase in $\delta^{18}O_{bul}$ preceded the 8 ka BP drop in $\delta^{18}O_{rub}$ and $\delta^{18}O_w$, which could point to upwelling starting slightly earlier than the completion of deglacial continental ice melting.

The $\Delta Tc_{rub-bul}$ record becomes increasingly positive in period III. Our data do not allow the distinction between a SW or NE monsoon cause. Previous studies, however, rather point to a weakening in NE monsoon strength (Bigg and Jiang, 1993) than an increase in SW monsoon. Conversely, the SW monsoon is reported to weaken in this period (Naidu and Malmgren, 1995; Overpeck et al., 1996; Naidu, 2004). The Holocene shift in $\Delta Tc_{rub-bul}$ could also represent a shift in seasonal abundance of *Globigerinoides ruber*, with more specimens calcifying in winter. This would increase the imprint of the summer–winter SST contrast on the $\Delta Tc_{rub-bul}$ record.

4.8. Comparison with previous work

A stepwise onset of the Holocene monsoon system has been previously described by several authors (Sirocko et al., 1993; Overpeck et al., 1996; Morrill et al., 2003; Williams et al., 2006). An increase in SW monsoon intensity at ~13 ka BP as seen in Core NIOP929 is also found in ODP723 (Naidu and Malmgren, 1996) and RC27 (Overpeck et al., 1996). The pronounced increase at 8 ka BP in Core NIOP929 is also found in 74KL (Sirocko et al., 1993) and several records from continental Africa (Adamson et al., 1980; Ritchie and Haynes, 1987; Stager, 1988). The variation in the number and timing of the steps may be explained by regional variations in climatic or oceanographic conditions. The shift in the monsoon proxy records at 8 ka BP, after which the monsoon intensity does not diminish, differs from the monsoon maximum at ~9 ka BP found by several workers (Prell, 1984; Sirocko et al., 1993). As the *Globigerina bulloides*/*Globigerinoides ruber* ratio in Core NIOP929 (Ivanova, 1999) reaches maximum values at 9 ka BP (Fig. 5), this difference in timing between the various records may also be due to a different response by the various proxies.

4.9. Seasonal SSTs

The seasonal SST records provide further insight into the temperatures that characterised the three monsoon periods described above. In period I, winter SST was generally ~1.5 °C lower than summer SST. This is indicative of a situation with stronger NE monsoon and weaker SW monsoon, which thus is not dominated by upwelling. In period II, summer and winter SST were similar at 25 to 26 °C. The difference with period II is largely due to an increase in winter SST. Surprisingly, winter insolation is at a minimum between these increases in T_{NE} at 12.5 and 8 ka BP (Fig. 5). The 8 ka BP shift coincides with a maximum in August insolation (Fig. 5). In period III, the large difference between the high (27 °C) winter and low (24 °C) summer SSTs indicates a modern day upwelling system.

The SW monsoon season SST is rather constant (at 26 °C) over a time period that covers the entire deglaciation and part of the interglacial (15 to 9 ka BP). It is possible that the global rise in temperature and the cooling effect of strengthened upwelling have cancelled each other out. Increased (summer) solar insolation (Fig. 5) could have warmed both the land and ocean surface. The higher heat capacity of the ocean could have resulted not only in the intra-annual but also an inter-annual lagged response to the insolation increase. This increases the ocean–continent pressure gradient, which in turn increases wind strength, and therefore upwelling. The dissimilarity of the winter SST and winter insolation records may be an indication of winter temperatures depending rather on glacial boundary conditions than on solar forcing. Winter SST was more variable than summer SST, possibly due to seasonally dependent forcing, or the absence of the previously described negative feedback mechanism. A similar pattern of stable summer SSTs and warm events in the winter SSTs is also found in the deglacial part of Core ODP 723A, located in the upwelling region off Oman (Naidu and Malmgren, 2005).

It is worth noting that all inferences from our calculations, taken at face value, are essentially unaltered when a threefold increase in winter calcification of *Globigerina bulloides* with respect to the modern day is assumed. Fig. 5 shows that the absolute temperatures and temperature gradients differ, but that the patterns through time are of similar shape. The method therefore appears not to be too sensitive to changes of this magnitude in seasonal distribution.

The calculated SSTs should not be interpreted as the maximum seasonal SST contrast, as *Globigerina bulloides* has its highest flux at the end of the upwelling season, when the temperature of the upwelled waters has already started to rise (Fig. 3) (Kroon and Ganssen, 1989; Peeters, 2000; Peeters et al., 2002).

5. Conclusions

In this study we present new data from Core NIOP929 from the Arabian Sea off Oman, which we have used in an attempt to reconstruct the seasonal SST history over the last 20 ka. From $\delta^{18}O$ of *Globigerina bulloides* and *Globigerinoides ruber*, and Mg/Ca of the latter, we inferred $\delta^{18}O_w$, $\Delta\delta^{18}O_{rub-bul}$, $\Delta Tc_{rub-bul}$ and Tc_{bul}. The difference in $\delta^{18}O$ of upwelling species *G. bulloides* and *G. ruber* ($\Delta\delta^{18}O_{rub-bul}$) can be converted to the difference in calcification temperatures ($\Delta Tc_{rub-bul}$), and is as such proposed as a proxy for seasonal SST contrast. In combination with Mg/Ca-derived SST it allows the quantification of seasonal SSTs. The proxy records thus constructed show that the period 20–0 ka BP can be subdivided into three different periods, representing different monsoon modes: I) A glacial monsoon mode (20–13 ka BP) characterised by weakly negative $\Delta Tc_{rub-bul}$ values, and SW monsoon SSTs (T_{SW}) that are higher than NE monsoon SSTs (T_{NE}). This pattern is indicative of a weaker SW monsoon, and stronger cooling by NE monsoon winds, compared to the modern situation. II) A transitional mode (13–8 ka BP) characterised by $\Delta Tc_{rub-bul}$ values oscillating around 0, and thus a strongly reduced seasonal SST contrast. (III) The modern monsoon mode started at 8 ka BP, with a shift of both seasonal SSTs of several degrees °C in less than 1000 years. The modern mode is characterised by highly positive $\Delta Tc_{rub-bul}$ values, a strong SW monsoon, and weak influence of the NE monsoon on SST.

The method proposed here is an attempt to quantify seasonal SSTs using a minimum amount of proxy data. The robustness of the approach can certainly be further improved, e.g. by additionally producing a Mg/Ca record of *Globigerina bulloides*, and by in situ observations on foraminiferal flux and intra-annual SST variability. Enhanced understanding of the ecology of the different species is essential to improve the method.

Acknowledgements

This manuscript greatly benefited from comments by P. Divakar Naidu and an anonymous reviewer, and the editors of this journal. Pallavi Anand is thanked for providing additional information on the uncertainty in the Mg/Ca vs temperature calibration. We thank Alex Wright for language advice.

References

Adamson, D.A., Gasse, F., Street, F.A., Williams, M.A.J., 1980. Late Quaternary history of the Nile. Nature 288 (5786), 50–55.

Altabet, M.A., Francois, R., Murray, D.W., Prell, W.L., 1995. Climate-related variations in denitrification in the Arabian Sea from sediment 15N/14N ratios. Nature 373, 506–509.

Anand, P., Elderfield, H., Conte, M.H., 2003. Calibration of Mg/Ca thermometry in planktonic foraminifera from a sediment trap time series. Paleoceanography 18 (2). doi:10.1029/2002PA000856.

Anderson, D.M., Prell, W.L., 1993. A 300 kyr record of upwelling off Oman during the Late Quaternary: evidence of the Asian southwest monsoon. Paleoceanography 8 (2), 193–208.

Barker, S., Greaves, M., Elderfield, H., 2003. A study of cleaning procedures used for foraminiferal Mg/Ca paleothermometry. Geochemistry, Geophysics, Geosystems 4 (9), 8407. doi:10.1029/2003GC000559.

Beaufort, L., et al., 1997. Insolation cycles as a major control of equatorial Indian Ocean primary production. Science 278, 1451–1454.

Bemis, B.E., Spero, H.J., Bijma, J., Lea, D.W., 1998. Reevaluation of the oxygen isotopic composition of planktonic foraminifera: experimental results and revised paleotemperature equations. Paleoceanography 13 (2), 150–160.

Berger, A.L., 1978. Long-term variations of daily insolation and Quaternary climatic changes. Journal of Atmospheric Sciences 35, 2362–2367.

Bigg, G.R., Jiang, D., 1993. Modeling the late Quaternary Indian Ocean circulation. Paleoceanography 8 (1), 23–46.

Brock, J.C., McClain, C.R., Anderson, D.M., Prell, W.L., Hay, W.W., 1992. Southwest monsoon circulation and environments of recent planktonic foraminifera in the northwestern Arabian sea. Paleoceanography 7 (6), 799–813.

Conan, S.M.-H., Brummer, G.J.A., 2000. Fluxes of planktic foraminifera in response to monsoonal upwelling on the Somalia Basin margin. Deep-Sea Research Part II: Topical Studies in Oceanography 47 (9–11), 2207–2227.

Curry, W.B., Ostermann, D.R., Guptha, M.V.S., Ittekkot, V., 1992. Foraminiferal production and monsoonal upwelling in the Arabian Sea: evidence from sediment traps. In: Summerhayes, C.P., Prell, W., Emeis, K.-C. (Eds.), Upwelling Systems: Evolution since the Miocene. Geological Society Special Publications. The Geological Society, London, pp. 93–106.

de Villiers, S., Greaves, M., Elderfield, H., 2002. An intensity ratio calibration method for the accurate determination of Mg/Ca and Sr/Ca of marine carbonates by ICP-AES. Geochemistry, Geophysics, Geosystems 3 (1). doi:10.129/2001GC000169.

Delaygue, G.E., et al., 2001. Oxygen isotope/salinity relationship in the northern Indian Ocean. Journal of Geophysical Research 106 (C3), 4565–4574.

Epstein, S., Buchsbaum, R., Lowenstam, H., Urey, H., 1953. Revised carbonate-water isotopic temperature scale. Geological Society of America Bulletin 64, 1315–1326.

Erez, J., Luz, B., 1983. Experimental paleotemperature equation for planktonic foraminifera. Geochimica et Cosmochimica Acta 47 (6), 1025–1031.

Fischer, J., Schott, F., Stramma, L., 1996. Currents and transports of the Great Whirl-Socotra Gyre system during the summer monsoon, August 1993. Journal of Geophysical Research 101 (C2), 3573–3587.

Fontugne, M.R., Duplessy, J.-C., 1986. Variations of the monsoon regime during the Upper Quaternary: evidence from carbon isotopic record of organic matter in North Indian Ocean sediment cores. Palaeogeography, Palaeoclimatology, Palaeoecology 56, 69–88.

Gupta, A.K., Anderson, D.M., Overpeck, J.T., 2003. Abrupt changes in the Asian southwest monsoon during the Holocene and their links to the North Atlantic Ocean. Nature 421, 354–356.

Ivanochko, T.S., et al., 2005. Variations in tropical convection as an amplifier of global climate change at the millennial scale. Earth and Planetary Science Letters 235 (1–2), 302–314.

Ivanova, E., 1999. Late Quaternary Monsoon History and Paleoproductivity of the Western Arabian Sea. Free University, Amsterdam. 172 pp.

Jung, S.J.A., Ganssen, G.M., Davies, G.R., 2001. Multidecadal variations in the early Holocene outflow of Red Sea water into the Arabian Sea. Paleoceanography 16 (6), 658–668.

Kim, S.-T., O'Neil, J.R., 1997. Equilibrium and nonequilibrium oxygen isotope effects in synthetic carbonates. Geochimica et Cosmochimica Acta 61 (16), 3461–3475.

Kroon, D., Ganssen, G.M., 1989. Northern Indian Ocean upwelling cells and the stable isotope composition of living planktonic foraminifers. Deep-Sea Research 36 (8), 1219–1236.

Kuhle, M., 1998. Reconstruction of the 2.4 million km^2 late Pleistocene ice sheet on the Tibetan Plateau and its impact on the global climate. Quaternary International 45–46, 71–108.

Levitus, S., Boyer, T.P., Antonov, J.I. 1994. World Ocean Atlas 1994, vol. 5, Interannual Variability of Upper Ocean Thermal Structure. Interannual Variability of Upper Ocean Thermal Structure. NOAA Atlas NESDIS 5 (U.S. Government Printing Office, Washington, DC).

Morrill, C., Overpeck, J.T., Cole, J.E., 2003. A synthesis of abrupt changes in the Asian summer monsoon since the last deglaciation. The Holocene 13 (4), 465–476.

Mortyn, P.G., Charles, C.D., 2003. Planktonic foraminiferal depth habitat and $\delta^{18}O$ calibrations: plankton tow results from the Atlantic sector of the Southern Ocean. Paleoceanography 18 (2), 1037.

Naidu, P.D., 2004. Isotopic evidences of past upwelling intensity in the Arabian Sea. Global and Planetary Change 40 (3–4), 285–293.

Naidu, P.D., Malmgren, B.A., 1995. A 2200 years periodicity in the Asian monsoon system. Geophysical Research Letters 22 (17), 2361–2364.

Naidu, P.D., Malmgren, B.A., 1996. A high-resolution record of late Quaternary upwelling along the Oman Margin, Arabian Sea based on planktonic foraminifera. Paleoceanography 11 (1), 129–140.

Naidu, P.D., Malmgren, B.A., 2005. Seasonal sea surface temperature contrast between the Holocene and last glacial period in the western Arabian Sea (Ocean Drilling Project Site 723A): modulated by monsoon upwelling. Paleoceanography 20 (1), A1004. doi:10.1029/2004PA001078.

Nair, R.R., et al., 1989. Increased particle flux to the deep ocean related to monsoons. Nature 338, 749–751.

Overpeck, J., Anderson, D., Trumbore, S., Prell, W., 1996. The southwest Indian monsoon over the last 18,000 years. Climate Dynamics 12, 213–225.

Peeters, F.J.C., 2000. The Distribution and Stable Isotope Composition of Living Planktic Foraminifera in Relation to Seasonal Changes in the Arabian Sea. Free University, Amsterdam. 184 pp.

Peeters, F.J.C., Brummer, G.-J.A., 2002. The seasonal distribution of living planktic foraminfera in the NW Arabian Sea. In: Clift, D.K.P., Gaedicke, C., Craig, J. (Eds.), The Tectonic and Climatic Evolution of the Arabian Sea Region. The Geological Society London, London, pp. 463–497.

Peeters, F.J.C., Brummer, G.-J.A., Ganssen, G., 2002. The effect of upwelling on the distribution and stable isotope composition of *Globigerina bulloides* and *Globigerinoides ruber* (planktic foraminifera) in modern surface waters of the NW Arabian sea. Global and Planetary Change 34, 269–291.

Prell, W.L., 1984. Variations of monsoonal upwelling: a response to changing solar radiation. In: Hansen, J., Takahashi, T. (Eds.), Climate Processes and Climate Sensitivity. Geophysical Monograph. American Geophysical Union, Washington D.C., pp. 48–57.

Prell, W.L., Campo, E.V., 1986. Coherent response of Arabian Sea upwelling and pollen transport to late Quaternary monsoonal winds. Nature 323, 526–528.

Prell, W.L., Murray, D.W., Clemens, S.C., Anderson, D.M., 1992. Evolution and variability of the Indian Ocean summer monsoon: evidence from the western Arabian sea drilling programme. Syntheses of results from scientific drilling in the Indian Ocean. Geophysical Monograph 70, 447–469.

Reichart, G.J., Lourens, L.J., Zachariasse, W.J., 1998. Temporal variability in the northern Arabian Sea oxygen minimum zone (OMZ) during the last 225,000 years. Paleoceanography 13 (6), 607–621.

Ritchie, J.C., Haynes, C.V., 1987. Holocene vegetation zonation in the eastern Sahara. Nature 330 (6149), pp. 645–647.

Russell, A.D., Spero, H.J., 2000. Field examination of the oceanic carbonate ion effect on stable isotopes in planktonic foraminifera. Paleoceanography 15 (1), 43–52.

Saher, M.H., Jung, S.J.A., H., E., Greaves, M.J., Kroon, D., in press. Western Arabian Sea SSTs during the last deglaciation.

Schott, F.A., McCreary, J., Julian, P., 2001. The monsoon circulation of the Indian Ocean. Progress in Oceanography 51 (1), 1–123.

Schulz, H., von Rad, U., Ittekkot, V., 2002. Planktic foraminifera, particle flux and oceanic productivity off Pakistan, NE Arabian Sea: modern analogues and application to the palaeoclimatic record. In: Clift, P.D., Kroon, D., Gaedicke, C., Craig, J. (Eds.), The Tectonic and Climatic Evolution of the Arabian Sea Region. The Geological Society of London, London, pp. 499–516.

Sirocko, F., et al., 1993. Century-scale events in monsoonal climate over the past 24,000 years. Nature 364, 322–324.

Smith, S.L., 2001. Understanding the Arabian Sea: reflections on the 1994–1996 Arabian sea expedition. Deep-Sea Research Part II: Topical Studies in Oceanography 48 (6–7), 1385–1302.

Spero, H.J., Bijma, J., Lea, D.W., Bemis, B.E., 1997. Effect of seawater carbonate concentration on foraminiferal carbon and oxygen isotopes. Nature 390 (6659), 497–500.

Stager, C.J., 1988. Environmental changes at Lake Cheshi, Zambia since 40,000 years B.P. Quaternary Research 29 (1), 54–65.

Van den Berg, J.B., et al., 2002. Reconstruction of sea surface temperatures from the oxygen isotope composition of fossil planktonic foraminifera. In: Hek, G.M. (Ed.), The Forty-second European Study Group with Industry. Shaker Publishing, pp. 91–120.

van Hinte, J.E., van Weering, T.C.E., Troelstra, S.R., 1995. Tracing a Seasonal Upwelling, vol. 4. National Museum of Natural History, Leiden.

Williams, M., et al., 2006. Abrupt return of the summer monsoon 15,000 years ago: new supporting evidence from the lower White Nile valley and Lake Albert. Dating the Quaternary: Progress in Luminescence Dating of Sediments. Quaternary Science Reviews, vol. 25(19–20), pp. 2651–2665.

Zhou, W., et al., 1996. Variability of monsoon climate in East Asia at the end of the last glaciation. Quaternary Research 46 (3), 219–229.